Acta Cryst. (1998). B**54**, 819–833

Distribution and Topology of the Electron Density in an Aluminosilicate Compound from High-Resolution X-ray Diffraction Data: the Case of Scolecite

Sandrine Kuntzinger, Nour Eddine Ghermani,* Yves Dusausoy and Claude Lecomte

Laboratoire de Cristallographie et Modélisation des Matériaux Minéraux et Biologiques, LCM3B, UPRES A CNRS 7036, Université Henri Poincaré, Nancy 1, Faculté des Sciences, Boulevard des Aiguillettes, BP 239, 54506 Vandoeuvre-lès-Nancy CEDEX, France. E-mail: ghermani@lcm3b.u-nancy.fr

(*Received 17 November 1997; accepted 9 March 1998*)

Abstract

The experimental electron density distribution in scolecite, $CaAl_2Si_3O_{10}.3H_2O$, has been derived from single-crystal high-resolution Ag $K\alpha$ X-ray diffraction data. A statistical method based on the prediction matrix has been used to discuss the estimation of the valence populations (P_{val}) in the kappa least-squares refinements. The densities on the Si—O—Si and Si—O—Al bridges have been characterized using the topology of the electron density through its Laplacian at the bond critical points. The Si—O and Al—O bond features are related to the atomic environment and to the Si—O—T geometries (T = Si, Al).

1. Introduction

The electron density distribution and related electrostatic properties are essential for an understanding of interatomic interactions in matter. Theoretical methods are becoming more and more precise in this field, but suffer mainly from the size of the system and necessitate approximations in order to reproduce the bulk properties. On the other hand, accurate high-resolution X-ray diffraction is an experimental technique that is able to accurately retrieve the electron density features between interacting atoms in the crystal. In the past decade, this experimental approach has shown its advantage and has permitted the calibratation of high-level quantum-mechanical calculations for the derivation of electrostatic properties of molecular compounds (Souhassou *et al.*, 1992; Pichon-Pesme *et al.*, 1992; Espinosa, Lecomte, Ghermani *et al.*, 1996). Using a multipolar density model, the electron density in the crystal is parametrized at the atomic level; therefore, all related properties such as atomic charges, electrostatic potential and field, and polarizability can be compared to theoretical calculations or other experimental results.

We are currently involved in the study of the electrostatic properties of zeolite-like aluminosilicate materials. The framework of these compounds, formed by SiO_4 and AlO_4 corner-linked tetrahedra in different geometries, gives rise to channels or large cavities in the solid state. In order to compensate for the negatively charged framework (formally due to the replacement of Si^{4+} by Al^{3+}), cations such as Li^+, Na^+ and Ca^{2+} are present in the crystal structure. These cations are linked to the O atoms of the framework and play an important role in the electrostatic and adsorption properties of the cavities, which make such materials of much industrial interest. In our previous study of natrolite (Ghermani *et al.*, 1996), $Na_2Al_2Si_3O_{10}.2H_2O$, we showed that the charge transfer between the Na^+ cation and the framework involves the nearest O atoms to this cation. A slightly more pronounced covalent character of the Si—O bond in comparison with Al—O was also reported in the same paper. In this study we are interested in the electron density distribution of a closely related natural zeolite, scolecite, $CaAl_2Si_3O_{10}.3H_2O$, in which the two sodium cations observed in natrolite are replaced by one calcium cation and one water molecule. Therefore, the symmetry of the crystal is reduced from *Fdd*2 to *F*1*d*1. A multipolar electron-density refinement against high-resolution X-ray diffraction data has been carried out successfully for this non-centrosymmetric compound. The hat matrix of the least-squares procedure (Prince & Nicholson, 1985; Antoniadis *et al.*, 1992; Prince & Boggs, 1992) was used in order to examine the influence of each observation on the model refinement, especially in the determination of the atomic net charges. The topological analysis of Bader (Bader & Essen, 1984; Bader *et al.*, 1984; Bader, 1990*a*,*b*) has been applied to the experimental electron density of scolecite in order to try to characterize more precisely the nature of the Si—O and Al—O bonds.

2. Experimental and methods

2.1. *Experimental*

A fragment with six bounding faces was cut from a large crystal of scolecite originating from Poona (India). It was chosen for its good crystal quality and for the well ordered Al, Si distribution as revealed by the electron microprobe analysis, which gave an Si/Al ratio equal to 1.5; no other cation than Ca^{2+} was detected. The crystalline sample is elongated along the *c* axis and displays (110), (1$\bar{1}$0) and (001) cleavage faces. Table 1 gives the conditions and details of the diffraction experiment. Scolecite crystallizes in the monoclinic space group *Cc*,

Table 1. *Experimental details*

Crystal data	
Chemical formula	$CaAl_2Si_3O_{10}.3H_2O$
Chemical formula weight	392.34
Cell setting	Monoclinic
Space group	*F*1*d*1 (*Cc*)
a (Å)	18.489 (2)
b (Å)	18.959 (2)
c (Å)	6.519 (1)
β (°)	90.611 (13)
V (Å^3)	2284.8 (5)
Z	8
D_x (Mg m^{-3})	2.28
Radiation type	Ag $K\alpha$
Wavelength (Å)	0.5609
No. of reflections for cell parameters	25
θ range (°)	10–28
μ (mm^{-1})	0.542
Temperature	Room
Crystal form	Parallelepiped
Crystal size (mm)	0.32 × 0.2 × 0.16
Crystal colour	Colourless
Data collection	
Diffractometer	Enraf–Nonius CAD-4
Data collection method	$\omega/2\theta$ scans
Absorption correction	Gaussian quadrature (De Titta, 1985) and empirical (Blessing, 1995)
T_{min}	0.864
T_{max}	0.924
No. of measured reflections	29 794
No. of independent reflections	9740
No. of observed reflections	6610
Criterion for observed reflections	$I > 3\sigma(I)$
R_{int}	0.0305
$(\sin\theta/\lambda)_{max}$ (Å^{-1})	1.28
Range of *h*, *k*, *l*	$-47 \rightarrow h \rightarrow 47$ $-48 \rightarrow k \rightarrow 48$ $-16 \rightarrow l \rightarrow 16$
No. of standard reflections	3
Frequency of standard reflections	Every 120 min
Refinement	
Refinement on	*F*
R	0.0265
wR	0.0237
S	0.85
No. of reflections used in refinement	6610
No. of parameters used	507
Weighting scheme	$w = 1/[\sigma^2(F^2) + (0.01F^2)^2]$
$(\Delta/\sigma)_{max}$	0.1
$\Delta\rho_{max}$ (e Å^{-3})	0.1
$\Delta\rho_{min}$ (e Å^{-3})	−0.2
Extinction method	Lorentzian isotropic type 1 (Becker & Coppens, 1974)
Extinction coefficient	0.41×10^4
Source of atomic scattering factors	*International Tables for X-ray Crystallography* (1974, Vol. IV)
Computer programs	
Data collection	*CAD*-4 (Enraf–Nonius, 1989)
Cell refinement	*CAD*-4 (Enraf–Nonius, 1989)
Data reduction	*DREADD* (Blessing, 1987, 1989)
Structure refinement	*MOLLY* (Hansen & Coppens, 1978)

but in order to compare it with the orthorhombic natrolite (*Fdd*2), the *F*1*d*1 (*Cc*) setting was chosen for scolecite (only the *d*-glide mirror perpendicular to **b** remains in this compound). The lattice parameters obtained in this study (Table 1) are slightly different from those derived from the neutron diffraction study of a crystal sample from Iceland [Joswig *et al.*, 1984; *a* = 18.508 (5), *b* = 18.980 (5), *c* = 6.527 (2) Å and β = 90.64 (1)°]. A total of 29 794 intensities were measured, consistent with the *F*1*d*1 space group and recorded as ω–2θ scan Bragg profiles up to a maximum reciprocal resolution of $s_{max} = (\sin\theta/\lambda)_{max} = 1.28$ Å^{-1}, in the following way: a complete sphere for $0 \leq s \leq 0.9$ Å^{-1} and a half-sphere ($k \geq 0$) for reflections belonging to the $0.9 \leq s \leq 1.28$ Å^{-1} range. Three reflections ($\bar{1}5,9\bar{1}$, $\bar{6}82$ and $97\bar{3}$) were chosen as standards to check the variation of the intensities and were measured every 2 h of the experiment. The reflections $\bar{1}1,13,\bar{1}$, $\bar{6}82$ and $10,14,\bar{2}$ were measured every 200 reflections to check any crystal disorientation. The total X-ray exposure time of the sample was 456 h.

2.2. *Data processing*

The program package *DREADD* (Blessing, 1987, 1989) was used to reduce the data and to perform the error analysis. A Lorentzian peak-width variation model was used to integrate the intensity profiles. The instrumental instability coefficient *p* (McCandlish *et al.*, 1975), based on the variation statistics of the standard reflection intensities, was found to be equal to 0.010 (1). The variance of each intensity was estimated as $\sigma^2(|F_o|^2) = [\sigma_c^2(|F_o|^2) + (p|F_o|^2)^2]$, where F_o is the observed structure factor and σ_c^2 is calculated using the propagation of error based on counting statistics and scan-angle uncertainty [$\sigma(\omega) = 0.005°$]. The absorption correction was performed using the Gaussian numerical integration in the program *ABSORB* (De Titta, 1985). The transmission factor *T* was found to be in the range 0.864–0.924. Moreover, in order to take into account the non-uniform irradiation of the crystal due to the monochromated inhomogeneous X-ray beam, the spherical harmonics empirical correction of Blessing (1995) was also applied. Since the space group of scolecite is non-centrosymmetric, anomalous-dispersion effects have to be taken into account. Sorting and averaging of the data were performed in point group *m*, giving rise to 12 959 reflections with $I > 3\sigma(I)$. These reflections were used in the first stages of the refinements. The enantiomorph polarity was checked using the program *SHELXL*93 (Sheldrick, 1993); the Flack parameter (Flack, 1983) value of −0.12 (3) indicates that no polarity problem occurs in scolecite.

2.3. *Pseudo-atom model*

The least-squares program *MOLLY* (Hansen & Coppens, 1978) was used to determine atomic coordi-

nates, displacement parameters and multipolar density coefficients. The form factors of neutral Si, Al, O and H atoms, and of the Ca^{2+} cation were calculated from Hartree–Fock wavefunctions (Clementi & Roetti, 1974). Anomalous-dispersion coefficients were from Cromer (1974). An isotropic extinction correction was included using the formalism by Thornley & Nelmes (1974) with extinction type 1 and a Lorentzian mosaic distribution.

In the Hansen–Coppens model (Hansen & Coppens, 1978) the electron density of the unit cell is considered as the superposition of pseudo-atomic electron densities. The pseudo-atom electron density is given by

$$\rho(\mathbf{r}) = \rho_{\text{core}}(r) + P_{\text{val}}\kappa^3\rho_{\text{val}}(\kappa r) + \sum_{l=0}^{l_{\max}} \kappa'^3 R_{n_l}(\kappa' r) \sum_{m=0}^{l} P_{\text{lm}} y_{\text{lm}\pm}(\theta, \varphi) \qquad (1)$$

where ρ_{core} and ρ_{val} are, respectively, Hartree–Fock spherical core and valence densities. In this aspherical density model, the refined valence population parameter P_{val} gives an estimation of the net atomic charge q with respect to the number of electrons N_{val} in the free atomic valence orbitals: $q = N_{\text{val}} - P_{\text{val}}$. The $y_{\text{lm}\pm}$'s are spherical harmonic angular functions of the order l in real form and $R_{n_l}(r)$ are Slater-type radial functions

$$R_{n_l}(r) = N_l r^{n_l} \exp(-\zeta r), \qquad (2)$$

where N_l is the normalization factor, and n_l and ζ are parameters depending, respectively, on the order l and on the atomic valence functions. P_{lm} are the multipolar population parameters of each associated spherical harmonic $y_{\text{lm}\pm}$, and κ and κ' are the contraction–expansion coefficients (Coppens *et al.*, 1979) for the spherical and multipolar valence densities, respectively.

The program *STATDENS* (Ghermani *et al.*, 1992), interfaced with a graphical tool, was used to calculate and map the static electron deformation density obtained by the multipolar refinements. The static deformation density is the difference between the multipolar model density (1) and the density of the procrystal, chosen as a reference, which constitutes the superposition of independent atomic densities (Clementi & Raimondi, 1963). These deformation density maps are expected to reveal noise-free static deformations of the atomic electron clouds owing to bond formation.

2.4. *Beyond the least-squares fit: influence and prediction*

In crystallographic studies of structures and electron densities the model parameters are derived from the observed amplitudes of structure factors $|F_o|$ by means of minimizing, in the least-squares method, the sum of the weighted residuals $\Delta = \Sigma w(K^{-1}|F_o| - |F_c|)^2$, where $w = 1/[\sigma^2(|F_o|)]$, $\sigma^2(|F_o|)$ being the variance of the observed structure factor, K^{-1} is the scale factor and F_c is the calculated structure factor. In order to improve the determination of the model parameters by the least-squares procedure, we have used a statistical method (Fedorov, 1972; Hoaglin & Welsh, 1978; Antoniadis *et al.*, 1992) based on the prediction matrix (also termed the hat matrix by statisticians) which relates the observations and the estimated structure factors. This method, which has been previously described for crystallographic refinements by Prince & Nicholson (1985) and Prince & Boggs (1992), was never referenced for charge density studies.

Given a set of m observations to be interpreted by a linear model with respect to n parameters, we obtain m linear equations which can be expressed in matrix form (Hamilton, 1964; Coppens, 1997) as

$$\mathbf{X}\Delta\mathbf{P} = \Delta\mathbf{F}, \qquad (3)$$

where $\Delta\mathbf{P} = (\mathbf{P}^1 - \mathbf{P}^0)$ is the n-dimensional vector of the changes of n parameters $\{\Delta p_j = p_j^1 - p_j^0\}_{j=1,n}$, $\Delta\mathbf{F} = (\mathbf{F}_o - \mathbf{F}_c^0)$ is the m-dimensional vector of the m differences $(K^{-1}|F_{o,\mathbf{h}_i}| - |F_{c,\mathbf{h}_i}(p_j^0)|)_{i=1,m}$, of the moduli of the observed and calculated structure factors at the Bragg vector $\mathbf{h}_i$ (i = 1,m) with the initial parameters $\{p_j^0\}_{j=1,n}$. In the case of the weighted least-squares procedure, $\mathbf{X}$ is the following $m \times n$ matrix

$$[X_{ij}] = w_{ii}^{1/2}[\partial F_{c,\mathbf{h}_i}/\partial p_j], \qquad (4)$$

with $w_{ii} = 1/[\sigma^2(|F_{oi}|)]$ and each element of $\Delta\mathbf{F}$ is replaced by $(K^{-1}|F_{o,\mathbf{h}_i}| - |F_{c,\mathbf{h}_i}|)/[\sigma(|F_{o,\mathbf{h}_i}|)]$. The least-squares normal equations are obtained by the transformation

$${}^t\mathbf{X}\mathbf{X}\Delta\mathbf{P} = {}^t\mathbf{X}\Delta\mathbf{F}, \qquad (5)$$

where ${}^t\mathbf{X}$ is the transposed matrix. The estimation $\Delta\mathbf{P}^{\text{est}}$ (by the least-squares method, starting with the values of p_j^0, p_j^1 is not exactly determined) of the change of parameters $\Delta\mathbf{P}$ is given by

$$\Delta\mathbf{P}^{\text{est}} = [{}^t\mathbf{X}\mathbf{X}]^{-1}{}^t\mathbf{X}\Delta\mathbf{F}. \qquad (6)$$

The symmetric matrix ${}^t\mathbf{X}\mathbf{X}$ may be ill-conditioned and may lead to irrelevant results. This case occurs when the determinant of the matrix approaches zero and thus the Gauss method for matrix inversion cannot be used. The Householder triangularization method (Lascaux & Theodor, 1986) is powerful in this case and gives more stable results (see, for example, Ghermani *et al.*, 1993). To reveal the ill-conditioning, the least-squares matrix is diagonalized in an orthogonal basis of a new set of parameters $\{p_j'\}_{j=1,n}$ and singularities appear through the near-zero diagonal elements. This singular value decomposition or eigenvalue filtering has been described by many authors (Watkin, 1994; Francl *et al.*, 1996, and references therein) and the problem of the ill-conditioning is overcome by imposing constraints on some parameters. These singularities, as pointed out in a recent study (El Haouzi *et al.*, 1996), are related to the lack of information on some parameters in the observed

data. It is thus necessary to analyse the data carefully in order to pick up which observations may contain the information on some parameters during the refinements. This point is important not only in relation to the model used, but also to the least-squares procedure. From the equations above

$$\mathbf{X}\Delta\mathbf{P}^{\text{est}} = \mathbf{X}[{}^t\mathbf{X}\mathbf{X}]^{-1}{}^t\mathbf{X}\Delta\mathbf{F} = \mathbf{H}\Delta\mathbf{F}, \tag{7}$$

where $\mathbf{H}$ is an $m \times m$ matrix defined by

$$\mathbf{H} = \mathbf{X}[{}^t\mathbf{X}\mathbf{X}]^{-1}{}^t\mathbf{X}. \tag{8}$$

Since $\mathbf{X}\mathbf{P}^0 = \mathbf{F}_c^0$, it is obvious that $\mathbf{H}\mathbf{F}_c^0 = \mathbf{F}_c^0$; consequently

$$\mathbf{X}\mathbf{P}^1 = \mathbf{F}_c^1 = \mathbf{H}\mathbf{F}_o \tag{9}$$

where $\mathbf{F}_c^1$ is the estimated vectorial value of $\mathbf{F}_o$. The $\mathbf{H}$ matrix projects the observation vector $\mathbf{F}_o$ on the n-dimensional space of solutions (Antoniadis *et al.*, 1992), (derivatives of parameters) where the estimated vector $\mathbf{F}_c$ lies. The $\mathbf{H}$ matrix is a projection matrix. Its elements H_{ij} denote the relation between the estimated value F^1_{c,h_i} and the observation F_{o,h_j}. This means that the estimation of F_{c,h_i} through the least-squares determination of the n parameters can be explained, in the statistical sense, by more than one observation (H_{ii} is lower than 1). H_{ii} represents the weight of the observation i on the prediction of F_{c,h_i}, then the matrix $\mathbf{H}$ is also termed the prediction matrix and H_{ii} is the leverage. The general properties (Antoniadis *et al.*, 1992) of the matrix elements H_{ij} are

$$\begin{aligned}
&\sum_{i=1}^{m} H_{ii} = n \text{ then the average value } \langle H_{ii}\rangle = n/m \\
&\quad 0 \le H_{ii} \le 1 \ \forall i \\
&-0.5 \le H_{ij} \le 0.5 \ \forall i \ne j \\
&\text{if } H_{ii} = 1 \text{ or } H_{ii} = 0 \text{ then } H_{ij} = 0 \ \forall \ i \ne j.
\end{aligned} \tag{10}$$

In crystallography the number of observations m is much larger than the number of parameters n to be determined, therefore, H_{ii} is, on average, very low. Velleman & Welsh (1981) have suggested that an observation with $H_{ii} > 3n/m$ [when $n > 6$ and $(m - n) > 12$] can be considered as influential on the fit by a least-squares procedure. In practice, during the refinements the calculations of H_{ii} reveal the observations which have a strong influence on the estimation of some parameters of the model. However, this analysis must only be carried out for parameters of the same kind. The same consideration applies to the singular value decomposition. Now if the H_{ii} value is high with respect to the threshold given by Velleman & Welsh (1981), the usual inspection of the deviates $e_i = K^{-1}|F_{o,\mathrm{h}_i}| - |F_{c,\mathrm{h}_i}|$ or weighted deviates $e_i/[\sigma(|F_{o,\mathrm{h}_i}|)]$ is an indicator of the eventual aberration of the observation F_{o,h_i}. However, we have to emphasize that an aberrant observation is not necessarily influential with respect to a given model and can be suppressed from the data without any change of the adjusted parameters.

2.5. *Refinement strategies*

With the data averaged in point group m, a series of high-order data ($0.9 \le s \le 1.28$ Å^{-1}) refinements was carried out in order to estimate the atomic coordinates and anisotropic displacement amplitudes U^{ij}. The starting atomic coordinates and equivalent isotropic displacement parameters were those determined from neutron diffraction data (Joswig *et al.*, 1984). The H atoms of the water molecules were refined isotropically using all data; then the O—H distances were kept fixed at 0.95 Å until the end of the multipolar refinement. The inspection of the residual Fourier maps† revealed anharmonic thermal motion features of the Ca^{2+} cation. Therefore, coefficients up to sixth order of the Gram–Charlier expansion (Kuhs, 1983) were refined for the Ca^{2+} cation.

The multipolar parameters are determined in local orthogonal atomic reference frames. For Si and Al atoms we have chosen orthogonal reference axes according to the (23) T^1 point group in order to reduce the number of multipole parameters. Thus, only the cubic harmonics [one octupole $l = 3$ and two hexadecapoles $l = 4$ with the constraint on the multipolar population $P_{44+} = 0.74P_{40}$ (Hansen & Coppens, 1978)] have been refined for these two atoms. For the O atoms of the framework, the x axis was chosen towards the Si or Al atoms with the y axis in the Si—O—Si or Si—O—Al planes and the z axis perpendicular to this plane. In water molecules, the x and y axes of the O atoms are directed towards the two H atoms. The H atoms have their x direction towards the O atom.

The pseudo-atom expansion was extended to octupoles ($l_{\max} = 3$) for O atoms, including those of the water molecule, and to dipoles ($l_{\max} = 1$) for H. The best radial functions of Si and Al atoms were obtained by inspection of the residual maps (Souhassou *et al.*, 1995), $n_l = 4$, 4, 4, 4 (l = 1–4); ζ's were taken from Clementi & Raimondi (1963): $\zeta_{\mathrm{Si}} = 1.614$ and $\zeta_{\mathrm{Al}} = 1.439$ Å^{-1}. For the O atoms $\zeta_{\mathrm{O}} = 2.381$ Å^{-1} and the multipole exponents were, respectively, $n_l = 2$, 2, 3 (l = 1–3). H atoms have $\zeta_{\mathrm{H}} = 1.196$ Å^{-1} and $n_l = 1$.

In the program *MOLLY* (Hansen & Coppens, 1978) the asymmetric unit is constrained to be neutral when P_{val} parameters are refined. In the case of scolecite the P_{val}'s of the water molecules have been refined separately from those of the framework in order to impose H_2O electroneutrality (a refinement allowing charge transfer led to unrealistic values). Therefore, no charge transfer was allowed between water molecules and the zeolite framework. The starting P_{val}'s for the ten O

† Supplementary data for this paper are available from the IUCr electronic archives (Reference: SH0112). Services for accessing these data are described at the back of the journal.

atoms of the framework were 6.2 e rather than 6 e in order to compensate for the charge of the calcium cation (2+), which was never refined.

The multipolar refinements were first carried out with all reflections, averaged in point group *m*, up to a resolution of $(\sin\theta/\lambda)_{\max} = 1.28$ Å^{-1}. We began the fit by imposing a chemical constraint on the atoms of the asymmetric unit starting with a natrolite-like constraint (Ghermani *et al.*, 1996) because, in first approximation, the pseudo-symmetry of natrolite (*Fdd*2) remains for the framework of scolecite. All atoms which are symmetry related in the natrolite space group were constrained to have the same electron density in scolecite. Two sets of parameters describe the three Si atoms, one for Si1 which lies near the cell origin and the other for the Si2 and Si3 atoms related by a pseudo-symmetry. In the same manner, electron density parameters of only one Al and five O atoms were considered (Al1 = Al2, O1 = O2, O3 = O4, O5 = O6, O7 = O8, O9 = O10). The three water molecules have been reduced to only two independent molecules, the first one corresponding to the two symmetry-related water molecules in the natrolite structure. The second water molecule replaces the sodium cation in natrolite. The chemical constraints were kept unchanged until the last refinements of the multipolar parameters and then they were removed. An isotropic extinction correction was applied during all the cycles of refinement; the final extinction parameter is $g = 0.41\,(2) \times 10^4$, which corresponds to a maximum intensity loss of 17% for the 351 reflection. At the convergence of the unconstrained refinements, the atomic positions and displacement parameters were relaxed and refined together with all multipolar parameters in the final cycles. Then the observed data were corrected for anomalous dispersion (Souhassou *et al.*, 1995), merged and averaged in Laue group 2/*m* [the internal agreement factors were $R_i(I) = 3.21\%$ before the correction and $R_i(I) = 3.05\%$ after the correction], and new cycles of refinement of all the parameters were carried out again to lead to the final results discussed here.

The atomic net charges, fundamental for the determination of electrostatic properties or in modelling, were determined from the kappa refinement (Coppens *et al.*, 1979). The best estimation of all structural parameters (especially the displacement parameters) originates from the multipolar refinements; the $P_{\rm lm}$ populations were set to zero and only the fitting of $P_{\rm val}$ and κ parameters was carried out.

At each stage of the refinements the diagonal elements of the hat matrix were calculated in order to detect the influential observations following the criterion of Velleman & Welsh (1981). Inspection of the residuals reveals those reflections which are aberrant. These aberrations decrease when the pseudo-atom model becomes more sophisticated (introduction of multipolar coefficients).

Final residual indices are given in Table 2. Table 3 lists the fractional coordinates and the final atomic anisotropic displacement amplitudes. $P_{\rm val}$, $P_{\rm lm}$, κ and κ' parameters of the multipolar electron density model (refinement 4′) and anharmonic thermal parameters for the calcium cation have been deposited.† In the residual electron density maps (Figs. 1*a* and 1*b*) the maxima and minima do not exceed 0.1 and −0.2 e Å^{-3}, respectively, which is satisfactory when compared with a crude estimation of experimental errors (Cruickshank, 1949; Rees, 1976)

$$\langle\sigma^2(\Delta\rho)\rangle^{1/2} = 2/V\left[\sum_{hi}(\sigma^2|F_{o,\mathrm{h}_i}|)\right]^{1/2} = 0.083 \text{ e Å}^{-3} \text{ and}$$

$$\langle\sigma^2_{\rm res}\rangle^{1/2} = 2/V\left[\sum_{hi}(K^{-1}|F_{o,\mathrm{h}_i}| - |F_{c,\mathrm{h}_i}|)^2\right]^{1/2} = 0.052 \text{ e Å}^{-3}.$$

Experimental deformation densities are given as supplementary material.† The prominent features are in close agreement with those observed in the static deformation map (see §3.2.).

2.6. *Topological analysis of the electron density*

As far as the refinement strategies described above ensure the deconvolution of the electron density from the thermal motion, the static electron density distribution, calculated directly using the multipolar coefficients, is able to retrieve accurately the basic characters of chemical bonds. Interatomic interactions are related to charge concentrations and depletions between the atoms in the crystal. This means that density features should be analysed through the gradient $\nabla\rho(\mathbf{r})$, the Laplacian $\nabla^2\rho(\mathbf{r})$ and the Hessian matrix $[\partial^2\rho/\partial x_i\partial x_j]$ of the electron density $\rho(\mathbf{r})$ (Bader & Essen, 1984; Bader, 1990*a*,*b*). The sites in the unit cell where the gradient value is zero localize the extrema (critical points denoted $\mathbf{r}_c$) and the eigenvalues (denoted λ_1, λ_2, λ_3) of the Hessian matrix at an extremum give the principal curvatures of the electron density. According to Bader (1990*a*,*b*), the Laplacian function $\nabla^2\rho(\mathbf{r})$ is related to the potential energy density $v(\mathbf{r})$ (negative) and the kinetic energy density $G(\mathbf{r})$ (positive) by

$$(\hbar^2/4m)\nabla^2\rho(\mathbf{r}) = 2G(\mathbf{r}) + v(\mathbf{r}). \qquad (11)$$

Thus, the sign of $\nabla^2\rho(\mathbf{r})$ is an indicator of the type of energy dominating at a given point **r**. $\nabla^2\rho(\mathbf{r}) < 0$ corresponds to a concentration of electrons at **r** and conversely $\nabla^2\rho(\mathbf{r}) > 0$ indicates a depletion at **r**. In order to characterize the chemical bonds we are interested in interatomic regions corresponding to (3,−1) bond

† See deposition footnote on p. 822.

Table 2. *Least-squares statistical factors R, wR and S of the different refinements*

$R(F) = \Sigma|(K^{-1}|F_o| - |F_c|)|/\Sigma K^{-1}|F_o|$; $wR(F) = [\Sigma w(K^{-1}|F_o| - |F_c|)^2/\Sigma wK^{-2}|F_o|^2]^{1/2}$; $S = [\Sigma w(K^{-1}|F_o| - |F_c|)^2/m - n]^{1/2}$, where $|F_o|$ and $|F_c|$ are, respectively, the modulus of the observed and the calculated structure factor, w the statistical weight, K^{-1} the scale factor, n the number of refined parameters and m the number of data.

Refinement number	$s = \sin\theta/\lambda$ (Å^{-1})	R	wR	S	n	m	Type of refinement
1	$0.0 \le s \le 1.28$	0.0377	0.0368	1.32	1	12 959	Spherical (m averaged data)
2	$0.0 \le s \le 1.28$	0.0341	0.0315	1.15	390	12 959	Multipolar C† (m averaged data)
2′	$0.0 \le s \le 1.28$	0.0337	0.0305	1.11	507	12 959	Multipolar NC‡ (m averaged data)
3	$0.0 \le s \le 1.28$	0.0325	0.0339	1.19	1	6610	Spherical (2/m averaged data)
4	$0.0 \le s \le 1.28$	0.0273	0.0253	0.92	390	6610	Multipolar C† (2/m averaged data)
4′	$0.0 \le s \le 1.28$	0.0265	0.0237	0.85	507	6610	Multipolar NC‡ (2/m averaged data)
5	$0.0 \le s \le 1.28$	0.0286	0.0285	1.00	24	6610	Kappa C† (2/m averaged data)
5′	$0.0 \le s \le 1.28$	0.0283	0.0267	0.94	41	6610	Kappa NC‡ (2/m averaged data)
6	$0.0 \le s \le 1.28$	0.0282	0.0261	0.92	41	6603	Kappa NC‡ without the seven reflections; see Table 6 (2/m averaged data)

† C = constrained refinement. ‡ NC = non-constrained refinement.

critical points for which the three eigenvalues of the Hessian matrix are non-zero and the algebraic sum of their signs is −1. The eigenvector associated with λ_3 is parallel to the bond path defined as the gradient line connecting the nuclei where the electron density has its maxima. The eigenvectors associated with λ_1 and λ_2 are perpendicular to the bond path. At the bond critical point $\mathbf{r}_c$, the value of the Laplacian $\nabla^2\rho(\mathbf{r}_c)$ is equal to the sum $\lambda_1 + \lambda_2 + \lambda_3$. In the case of (3,−1) critical points, λ_3 is positive and λ_1 and λ_2 are negative. A covalent bond or shared interaction such as a C—C or a C—N bond is characterized by a negative Laplacian [$\nabla^2\rho(\mathbf{r}_c)$ is around −17 e Å^{-5} for a C—C bond and −15 e Å^{-5} for a C—N bond (Stewart, 1991; Espinosa, Lecomte, Molins *et al.*, 1996)] and a high value of the density $\rho(\mathbf{r}_c)$ ($\sim$ 2 e Å^{-3}) is expected at the bond critical point. In this case the magnitude of $|\lambda_1|$, where $|\lambda_1| > |\lambda_2|$, is larger than $|\lambda_3|$, corresponding to a concentration of the electron density between the bonded atoms. In other words, the potential energy density in (11) is dominating. On the other hand, a closed-shell interaction will have a positive value of the Laplacian and a low electron density (less than 0.5 e Å^{-3}) at the bond critical point (intermolecular bonds, ionic interactions). The Pauli principle, related to the kinetic energy, dominates this type of interaction (Bader, 1990*a*,*b*), yielding a repulsion of the electrons towards the nuclei, thus a depletion of the electron density at the bond critical point. The ratio $|\lambda_1|/|\lambda_3|$ is expected to be less than 1 for these closed-shell interactions. However, intermediate values of these features may also be encountered and are attributed to a mixed character of the bond (Espinosa *et al.*, 1998).

3. Results and discussion

3.1. *Structure of scolecite and comparison with natrolite*

Many authors have been interested in the structure of scolecite (Fälth & Hansen, 1979; Joswig *et al.*, 1984; Kvick *et al.*, 1985) and room- and low-temperature X-ray and neutron diffraction experiments have been carried out. A selected set of bond lengths and angles in scolecite obtained after multipolar refinement 4′ (Table 2) is given as supplementary material.† These values are in good agreement with those calculated from the atomic coordinates in the neutron diffraction study of Joswig *et al.* (1984). The framework of scolecite is isotypic with that of natrolite, slightly distorted owing to the replacement of the two Na^+ cations of natrolite by one Ca^{2+} and one water molecule (O*w*3) in scolecite. As in natrolite, the structure of scolecite presents parallel channels along the *c* axis containing the Ca^{2+} cations, and O*w*1 and O*w*2 are the symmetry-related water molecules in natrolite (Fig. 2). The aluminosilicate framework results from oxygen-connected four-membered rings of tetrahedra. A quarter of the ring is composed of a central silicon tetrahedron surrounded by two opposing pairs of SiO_4 and AlO_4 tetrahedra. Owing to the *F*-centring mode and the *d*-glide mirror plane at (x, 1/8, z), these quarter units are periodically reproduced by a pseudo-2_1 screw axis parallel to **c**. Except for the central silicon tetrahedron, all silicon or aluminium tetrahedra are surrounded by, respectively, three aluminium and one silicon tetrahedra or three silicon and one aluminium tetrahedra. In the two compounds the water molecules are bound to the aluminosilicate framework by hydrogen bonds, the strongest involving the O2 and H32 (O*w*3) atoms [O2$\cdots$H32 = 1.7518 (8) Å] in scolecite. On the other hand, compared with natrolite, the compensation of the negatively charged framework in scolecite is ensured by the formal positive 2+ charge of the calcium cation. The periodic units of the framework along the *c* axis in natrolite and scolecite are almost equal. The calcium cation sits on one of the two sites of sodium of the former compound. Therefore, in scolecite the pseudo-2_1-axis-related O atoms of the framework see alternatively one Ca^{2+} cation and one neutral water molecule, and thus on

† See deposition footnote on p. 822.

Table 3. *Fractional atomic coordinates, equivalent isotropic displacement parameters ($Å^2$) and anisotropic displacement amplitudes U^{ij}*

$$U_{eq} = (1/3)\Sigma_i\Sigma_j U^{ij} a^i a^j \mathbf{a}_i.\mathbf{a}_j.$$

	x	y	z	U_{eq}
Si1	0.0	0.00440 (1)	0.0	0.0061
Si2	0.14988 (2)	0.20684 (1)	0.62016 (6)	0.00583
Si3	−0.16554 (2)	−0.20757 (1)	0.62541 (6)	0.00583
Al1	0.03301 (2)	0.09166 (2)	0.61111 (6)	0.0059
Al2	−0.04989 (2)	−0.08706 (2)	0.61566 (6)	0.00625
O1	0.01582 (5)	0.07447 (4)	0.86835 (12)	0.01097
O2	−0.01686 (5)	−0.06206 (4)	0.85576 (13)	0.01206
O3	0.07063 (4)	0.17453 (4)	0.57520 (12)	0.0084
O4	−0.08723 (4)	−0.17095 (4)	0.64018 (13)	0.00879
O5	0.09212 (4)	0.02618 (4)	0.52445 (13)	0.01053
O6	−0.10760 (5)	−0.02037 (4)	0.53075 (13)	0.01215
O7	0.20442 (4)	0.14616 (4)	0.70868 (13)	0.011
O8	−0.23048 (4)	−0.15649 (4)	0.68706 (13)	0.01147
O9	0.18249 (5)	0.23368 (5)	0.40244 (13)	0.01229
O10	−0.17813 (4)	−0.23524 (4)	0.38923 (12)	0.01073
Ca	0.22398 (2)	0.01820 (1)	0.61487 (5)	0.01066
O*w*1	0.03037 (9)	0.20119 (6)	0.0629 (2)	0.03308
O*w*2	−0.05422 (7)	−0.20473 (7)	0.1629 (2)	0.02871
O*w*3	0.06283 (6)	0.32038 (5)	0.3578 (2)	0.02465
H11	0.02405	0.16035	−0.01973	0.04023
H12	0.05935	0.23207	−0.01574	0.04873
H21	−0.0916	−0.2196	0.25195	0.03301
H22	−0.02417	−0.17535	0.24588	0.05306
H31	0.10722	0.32241	0.28559	0.0364
H32	0.04359	0.3668	0.35317	0.03909

	U^{11}	U^{22}	U^{33}	U^{12}	U^{13}	U^{23}
Si1	0.00714 (8)	0.00687 (8)	0.00429 (8)	0.00014 (7)	0.00009 (6)	−0.00013 (7)
Si2	0.00489 (8)	0.00633 (8)	0.00625 (9)	−0.00064 (7)	−0.00042 (6)	−0.00035 (7)
Si3	0.00538 (8)	0.00621 (8)	0.00591 (8)	−0.00086 (7)	0.00040 (6)	0.00020 (7)
Al1	0.00645 (10)	0.00521 (9)	0.00603 (10)	−0.00011 (8)	−0.00035 (8)	−0.00013 (8)
Al2	0.00694 (10)	0.00544 (9)	0.00638 (10)	−0.00084 (8)	0.00011 (8)	0.00038 (8)
O1	0.01699 (29)	0.00843 (22)	0.00753 (23)	−0.00043 (20)	0.00162 (20)	0.00208 (18)
O2	0.01798 (32)	0.00926 (22)	0.00884 (24)	−0.00019 (21)	−0.00428 (22)	−0.00316 (20)
O3	0.00592 (19)	0.00668 (19)	0.01256 (25)	−0.00174 (15)	−0.00200 (17)	0.00118 (17)
O4	0.00711 (20)	0.00714 (20)	0.01211 (25)	−0.00276 (16)	−0.00032 (17)	0.00089 (17)
O5	0.01108 (24)	0.00824 (22)	0.01227 (26)	0.00245 (18)	−0.00043 (19)	−0.00421 (19)
O6	0.01259 (26)	0.01138 (25)	0.01251 (27)	0.00360 (21)	0.00175 (21)	0.00581 (21)
O7	0.00851 (22)	0.01026 (23)	0.01411 (27)	0.00239 (18)	−0.00546 (19)	−0.00056 (20)
O8	0.00997 (23)	0.01240 (26)	0.01213 (26)	0.00294 (20)	0.00373 (19)	−0.00024 (21)
O9	0.01055 (24)	0.01698 (29)	0.00941 (25)	−0.00153 (22)	0.00364 (19)	0.00120 (22)
O10	0.00816 (21)	0.01749 (29)	0.00651 (22)	−0.00047 (20)	−0.00156 (17)	−0.00336 (20)
Ca	0.01040 (6)	0.01143 (6)	0.01012 (7)	−0.00086 (5)	−0.00087 (5)	−0.00123 (6)
O*w*1	0.05367 (85)	0.02130 (47)	0.02456 (52)	−0.00610 (52)	0.01784 (54)	−0.00982 (40)
O*w*2	0.02719 (52)	0.03906 (70)	0.02009 (46)	−0.00773 (48)	0.01034 (39)	−0.01041 (46)
O*w*3	0.01510 (35)	0.01373 (34)	0.04505 (71)	0.00110 (28)	−0.00359 (39)	0.00385 (39)
H11	0.040 (7)					
H12	0.049 (8)					
H21	0.033 (7)					
H22	0.053 (10)					
H31	0.036 (10)					
H32	0.039 (10)					

average a charge of 1+, as in natrolite. From the observed bond lengths and angles in the structures of natrolite and scolecite, some systematic features can be observed. Table 4 gives the average values of these parameters in the two compounds with respect to the coordination number (CN) of the framework O atoms. Experimental geometrical parameter values for silicates (Hill & Gibbs, 1979) are also reported in Table 4 for the sake of comparison. In silicates, according to Liebau (1985), the Si—O bond distance increases with the coordination number (CN) of the O atoms. This feature can be ascribed to a decrease of the attraction (the Si—O bond energy is lower) between Si and O when several cations (or protons in hydrogen bonds) are in the vici-

nity of the silicon bound to an O atom. The Si—O bond lengths in the natrolite and scolecite structures adopt this feature whenever the O atom is involved in Si—O—Si or Si—O—Al bridges (Table 4). Conversely, the Al—O bond distances do not exhibit any relationship with the CN values as shown in Table 4. In scolecite, the comparison of Si—O—Si and Si—O—Al bond angles shows that the mean angle ⟨Si—O—Si⟩ of 142 (8)° (for all mean values the e.s.d. is calculated as the square root of the variance of the angle distribution) is larger than the corresponding ⟨Si—O—Al⟩ of 135 (4)°. For the sake of comparison, the Si—O—Si and ⟨Si—O—Al⟩ angles are equal to 144.31 (6) and 136 (4)° in natrolite, respectively. However, the Si—O—Si mean angles increase when the coordination number of the O atoms decreases: Si—O(H)—Si 134.05 (5)° (scolecite) and Si—O(H)—Si 144.31 (5)° (natrolite) for CN = 3; Si—O—Si 150.79 (6)° (scolecite) for CN = 2. The Si—O—Al mean angles also increase with the decrease of the coordination number: for CN = 3, ⟨Si—O(H)—Al⟩ 139 (4)° (scolecite), ⟨Si—O(Na^+)—Al⟩ 137 (2)° (natrolite), ⟨Si—O(Ca^{2+})—Al⟩ 133 (4)°; for CN = 4, ⟨Si—O(2Na^+)—Al⟩ 129.84 (4)° (natrolite). These features have already been observed in a statistical survey of the geometry of silicates and are in agreement with the results of molecular-orbital calculations reported by Hill & Gibbs (1979).

The *T*—O—*M* angles (*T* = Si, Al; *M* = Na^+, Ca^{2+}) are distributed in two groups, corresponding to values around 95 and 125°, probably due to two bond-energy minima (Table 4). In scolecite the CN of the Ca^{2+} cation is seven and the resulting coordination polyhedron is a distorted pentagonal bipyramid, as reported by Fälth & Hansen (1979). As shown in Table 4, the sum of the *T*—O—*M* angles is close to 360°. This means that the O atoms are almost in the plane containing the Si and Al atoms, and the Ca^{2+} cation. Moreover, the Ca^{2+}—O bond lengths are larger for the O atoms belonging to the framework tetrahedra [mean value 2.53 (4) Å] than for those of the water molecules [mean value 2.34 (2) Å]. The smallest value of the O—Ca^{2+}—O angle is obtained for O atoms of the same Si or Al tetrahedron and the

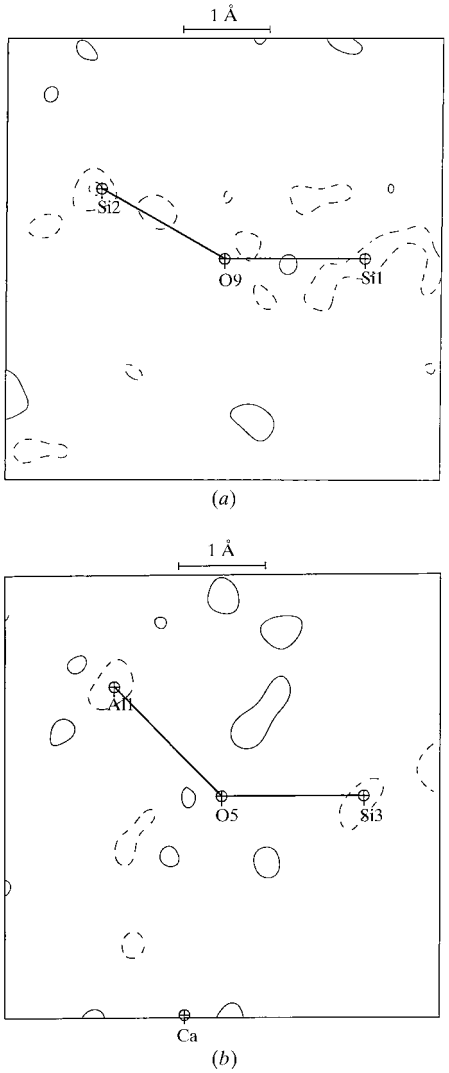

Fig. 1. Residual density in (*a*) the Si1—O9—Si2 and (*b*) the Si3—O5—Al1 planes of scolecite after the multipolar refinement 4′. Contour intervals ±0.1 e $Å^{-3}$; negative contours dashed; zero contour omitted (Fourier summation over data with $0 \le s \le 0.9$ $Å^{-1}$).

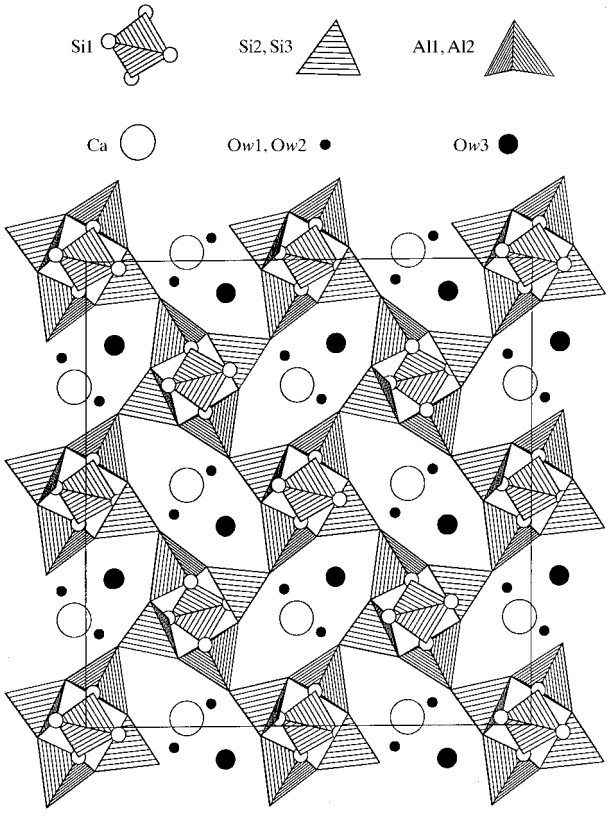

Fig. 2. View of the structure of scolecite along the *c* axis (*STRUPLO*90; Fischer *et al.*, 1991).

Table 4. *Comparison between the structural parameters of scolecite and natrolite*

Mean values of interatomic distances $\langle d(\mathrm{Si-O})\rangle$ in Å. The e.s.d.'s of the mean values are calculated as the square roots of the variances of the bond-length distributions.

	CN	Scolecite	Natrolite[a]
$\langle d(\mathrm{Si-O})\rangle$ in Si—O—Si		1.633 (9)	1.634 (3)
$\langle d(\mathrm{Si-O})\rangle$ in Si—O—Al		1.611 (11)	1.613 (5)
$\langle d(\mathrm{Si-O})\rangle$ in Si—O—Si	2	1.624 (5)	
$\langle d(\mathrm{Si-O})\rangle$ in Si—O(H)—Si	3	1.641 (5)	1.634 (3)
$\langle d(\mathrm{Si-O})\rangle$ in Si—O—Al	2	1.600 (3)	
$\langle d(\mathrm{Si-O})\rangle$ in Si—O(H)—Al	3	1.605 (5)	1.6056 (8)
$\langle d(\mathrm{Si-O})\rangle$ in Si—O(Ca,Na)—Al	3	1.620 (10)	1.6127 (6)
$\langle d(\mathrm{Si-O})\rangle$ in Si—O(2Na)—Al	4		1.6193 (8)

Correlation between d(Si—O) bond lengths and Si—O—Si angles.

Compound		Angle (°)	Bond length (Å)
Silicates[b]		130	1.655
Scolecite	Si1—O10(H)—Si3	134.05 (5)	1.6418 (7) and 1.6409 (8)
Silicates[b]		140	1.634
Natrolite[a]	Si1—O5(H)—Si2	144.31 (5)	1.6310 (9) and 1.6368 (9)
Silicates[b]		150	1.622
Scolecite	Si2—O9—Si1	150.79 (6)	1.6295 (8) and 1.6196 (8)

T—Si—M angles (°) (T = Si, Al; M = Al, Ca^{2+}, Na^{+}).

Scolecite	O7	O3	O5	O4
Si—O—Al	127.48 (5)	133.19 (4)	135.06 (5)	138.27 (5)
Si—O—Ca	132.88 (4)	125.44 (4)	99.80 (3)	96.53 (3)
Al—O—Ca	98.19 (3)	100.53 (3)	125.14 (4)	121.83 (4)
Σ angles	358.55 (12)	359.16 (11)	360.00 (12)	356.63 (12)
Natrolite[a]	O2	O2	O4	O3
Si—O—Al	129.84 (4)	129.84 (4)	135.00 (5)	138.70 (4)
Si—O—Na	128.04 (4)	89.69 (3)	125.67 (5)	99.12 (3)
Al—O—Na	91.49 (3)	123.46 (3)	95.81 (3)	119.21 (4)
Σ angles	349.37 (11)	342.99 (10)	356.48 (13)	357.03 (11)

Notes: (*a*) Ghermani *et al.* (1996); correlation with the coordinaton number (CN) and systematic features in silicates; (*b*) Hill & Gibbs (1979).

interaction with the Ca^{2+} cation induces a distortion inside the tetrahedron of the smallest O—(Si,Al)—O angles: O4—Ca^{2+}—O5 59.67 (3)° for O4—Si3—O5 103.68 (4)°, and O3—Ca^{2+}—O7 63.39 (4)° for O3—Al1—O7 97.72 (4)°. The other O—Ca^{2+}—O angles are larger than 80°. In natrolite the Na^{+} cation is bound to six O atoms: to four framework O atoms (2 × O2, O3 and O4) and two O atoms from the water molecules (not reported in Table 4). As in scolecite, the Si—O—Na^{+} and Al—O—Na^{+} angles have values around 95 and 125° (Table 4). The natrolite oxygen O2 linked to two Na^{+} cations exhibits a different geometry than that of O3 and O4 bound to only one Na^{+}. The Na^{+}—O bond length is larger for O2 [Na^{+}—O2 2.5181 (8) and 2.6149 (8) Å] than for O3 and O4 [Na^{+}—O3 2.367 (2) and Na^{+}—O4 2.3948 (8) Å]. These latter values are comparable to the Na^{+}—Ow bond distances in natrolite [Na^{+}—Ow1 2.371 (2) and Na^{+}—Ow2 2.394 (2) Å]. As in scolecite, the lower values of the O—Na^{+}—O angles correspond to the O atoms belonging to the same Si or Al tetrahedron [O2—Na^{+}—O4 68.06 (3)° for O2—Al—O4 104.12 (3)°, and O2—Na^{+}—O3 62.81 (2)° for O2—Si2—O3 107.41 (3)°]. The other O—Na^{+}—O angles are larger than 80°.

3.2. *Static deformation electron density*

In scolecite we have considered Si—O and/or Al—O bonds in two groups: the first group corresponds to an O atom involved in a Si—O—Si bond, the second group is

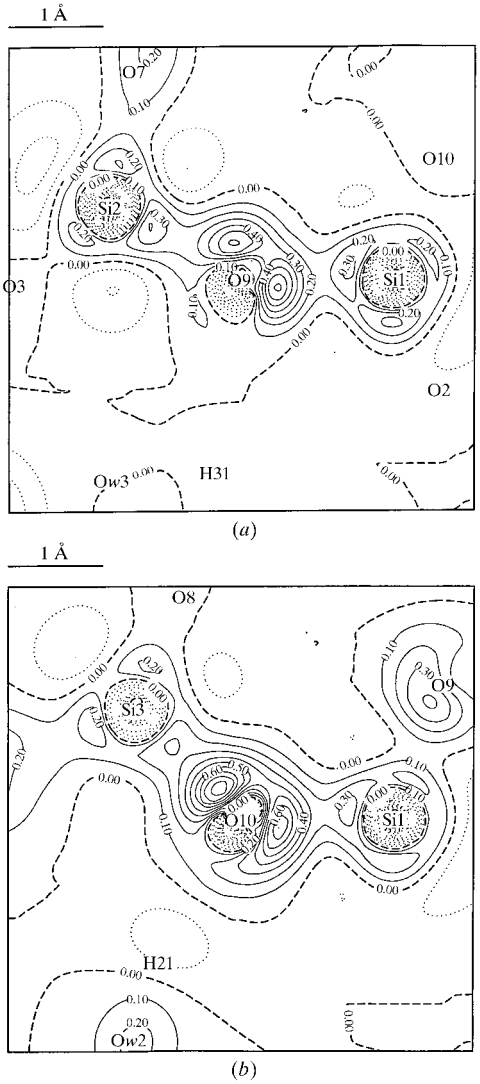

Fig. 3. Static deformation density in the Si—O—Si bridge planes (*a*) Si1—O9—Si2 and (*b*) Si1—O10—Si3. Contour intervals ±0.1 e Å^{-3}; negative contours dashed. H31 and H21 are, respectively, −1.04 and 0.50 Å from the plane.

for an O atom which links one Si atom and one Al atom. The atomic environment and local geometrical features have to be taken into account in order to make a comparison between the significant features of the electron deformation density. As reported in our previous study of natrolite (Ghermani *et al.*, 1996), the main feature of the deformation densities is a concentration of charge around the O atoms and a more or less pronounced electron depletion near the Si or Al atoms. Fig. 3 shows the static electron deformation densities of the first group in the Si1—O9—Si2 (Fig. 3*a*) and Si1—O10—Si3 (Fig. 3*b*) planes, where Si1 is the Si atom near the origin. In the Si1—O9—Si2 bridge [Si1—O9—Si2 150.79 (6)°] the density peak height values are 0.70 [Si1—O9 1.6196 (8) Å] and 0.60 e Å^{-3} [Si2—O9 1.6295 (8) Å]. Both peaks are localized at 0.45 Å from the O9 atom. The electron density peaks in the bonds of the Si1—O10—Si3 bridge [Si1—O10—Si3 134.05 (5)°] are 0.8 to 0.9 e Å^{-3} at 0.45 Å from O10 [Si1—O10 1.6418 (7) and Si3—O10 1.6409 (8) Å]. If we compare these two bridges, the electron deformation density has a tendency to be shifted towards the interior of the Si—O—Si angle in Si1—O9—Si2. The same observation has been made in natrolite for an Si—O—Si angle of 144.31 (6)°. This feature is also in agreement with the results of theoretical calculations of Gibbs *et al.* (1997) and with their comparison with experimental results for coesite (Downs, 1994). These authors have studied the Si—O bond in several molecules and have shown that the polarizability of the electron density in such a bond increases when the Si—O—Si angle opens, which implies a shortening of the Si—O bond distance (Gibbs *et al.*, 1997). Furthermore, in scolecite the interaction of these two Si—O—Si bridges with the water molecules involves the O10 atom [O10—H21 (O*w*2) 1.8652 (8) Å (H21 is 0.5 Å above the Si1—O10—Si3 plane)] more strongly than O9 [O9—H31 (O*w*3) 2.3076 (9) Å]. This feature is reproduced by a slight polarization of the lone-pair densities of the O10 atom towards the H atom. To describe the Si—O—Al bridges we have selected in Fig. 4 the static electron deformation density in the Si1—O1—Al1 (Fig. 4*a*), Si1—O2—Al2 (Fig. 4*b*) and Si2—O3—Al1 (Fig. 4*c*) planes. In these cases also, the electron deformation density is concentrated around the O atoms with visible polarization of their lone pairs either in the presence of hydrogen bonds [O1—H11 (O*w*1) 1.7900 (8), O2—H32 (O*w*3) 1.7518 (8) Å, compared with O—H 1.8871 (8) Å in natrolite] or due to a strong interaction with a cation [O3—Ca^{2+} 2.4900 (7) Å, compared with O—Na^{+} 2.367 (2) Å for the nearest oxygen to Na^{+} in natrolite]. This last feature has also been observed in forsterite (van der Val & Vos, 1987) between one of the O atoms of an SiO_4 tetrahedron and the Mg^{2+} cation. In the Si—O—Al bridges of scolecite, the electron density peak heights are 0.8 e Å^{-3} for Si1—O1 [Si1—O1 1.6101 (8) Å], 1.0 e Å^{-3} for Si2—O3 [Si2—O3 1.6121 (7) Å] and 1.2 e Å^{-3} for Si1—O2 [Si1—O2

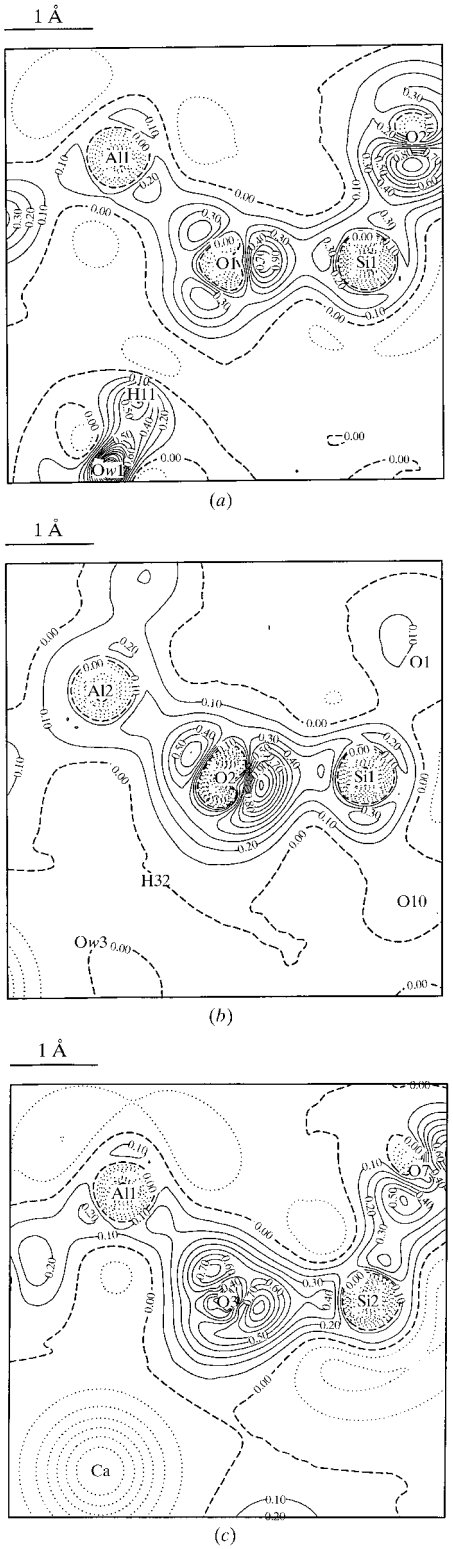

Fig. 4. Static deformation density in the Si—O—Al bridge planes (*a*) Si1—O1—Al1, (*b*) Si1—O2—Al2 and (*c*) Si2—O3—Al1. Contours as in Fig. 3. H11 and H32 are, respectively, +0.09 and −0.97 Å, and Ca^{2+} +0.44 Å from the planes.

Table 5. *The Laplacian $\nabla^2\rho(\mathbf{r}_c)$, eigenvalues of the Hessian matrix λ_1, λ_2 and λ_3, ratio $|\lambda_1/\lambda_3|$, electron density $\rho(\mathbf{r}_c)$ at the bond critical points (CP) $\mathbf{r}_c$ and distances d_1 and d_2 [d_1 = CP—T (T = Si, Al, Ca) and d_2 = O—CP]*

Bonds	d_1 (Å)	d_2 (Å)	$\nabla^2\rho(\mathbf{r}_c)$ (e Å^{-5})	$\rho(\mathbf{r}_c)$ (e Å^{-3})	λ_1	λ_2	λ_3	$\lvert\lambda_1/\lambda_3\rvert$
Si1—O2	0.68	0.92	20.96	1.17	−8.24	−7.69	36.89	0.223
Si1—O1	0.70	0.91	17.79	1.06	−7.59	−6.95	32.33	0.235
Si1—O9	0.71	0.91	16.78	0.96	−6.45	−5.87	29.10	0.222
Si1—O10	0.71	0.93	15.82	0.96	−6.32	−5.95	28.09	0.225
Si2—O6	0.69	0.91	17.51	1.01	−7.12	−6.91	31.54	0.226
Si2—O3	0.69	0.92	18.54	1.03	−7.60	−7.40	33.54	0.227
Si2—O9	0.71	0.92	15.05	0.89	−5.89	−5.71	29.66	0.199
Si2—O7	0.71	0.93	15.89	0.94	−6.65	−6.46	29.01	0.229
Si3—O4	0.70	0.91	17.11	1.02	−6.45	−5.94	29.50	0.218
Si3—O8	0.70	0.90	17.87	1.03	−6.39	−6.25	30.51	0.209
Si3—O5	0.70	0.93	16.27	0.99	−6.28	−5.86	28.41	0.221
Si3—O10	0.70	0.94	17.07	0.99	−6.02	−6.00	29.08	0.207
Al1—O3	0.76	0.97	15.85	0.59	−4.37	−3.86	24.09	0.181
Al1—O1	0.77	0.97	15.00	0.55	−3.92	−3.53	22.45	0.175
Al1—O5	0.77	0.98	14.11	0.60	−4.30	−4.10	22.50	0.191
Al1—O7	0.77	0.99	14.48	0.54	−4.10	−3.47	22.05	0.186
Al2—O2	0.76	0.98	14.67	0.72	−4.61	−4.22	23.49	0.196
Al2—O6	0.76	0.98	14.19	0.70	−4.66	−4.56	23.41	0.199
Al2—O4	0.76	0.98	14.03	0.71	−4.55	−4.42	23.01	0.198
Al2—O8	0.78	0.96	13.17	0.61	−3.54	−3.32	20.02	0.177
Ca···O3	1.23	1.26	3.16	0.15	−0.68	−0.65	4.50	0.151
Ca···O5	1.24	1.27	2.99	0.14	−0.64	−0.58	4.21	0.152
Ca···O7	1.27	1.26	2.64	0.12	−0.54	−0.52	3.70	0.146
Ca···O4	1.28	1.33	2.43	0.12	−0.50	−0.46	3.39	0.147
Ca···O*w*1	1.17	1.14	4.55	0.21	−1.07	−0.98	6.60	0.162
Ca···O*w*2	1.19	1.16	4.19	0.20	−1.00	−0.87	6.07	0.165
Ca···O*w*3	1.18	1.17	4.44	0.21	−1.08	−0.97	6.49	0.166

1.6008 (8) Å]. In the Al—O bonds the peak heights vary from 0.4 [Al1—O1 1.7409 (8) Å] to 0.7 e Å^{-3} [Al1—O3 1.7349 (7), Al2—O2 1.7399 (8) Å]. The angle Si1—O2—Al2 [143.82 (5)°] is larger than Si1—O1—Al1 [134.75 (5)°] and Si2—O3—Al1 [133.19 (4)°]. In comparison to the Si—O—Si bridges, the Si—O bonds are shorter on average when the O atom is bound to an aluminium, the shortest being Si1—O2 1.6008 (8) Å, corresponding to the highest Si—O—Al angle [Si1—O2—Al2 143.82 (5)°]. Thus, as observed for the Si—O—Si bridge, the polarizability of the Si—O bond in Si—O—Al is enhanced with angle opening (Si1—O2—Al2 bond). On average, the Al—O electron density peaks are lower (0.4–0.8 e Å^{-3}) than those found in the Si—O link.

3.3. *The Laplacian and topology of the electron density*

In order to characterize the Si—O and Al—O bonds we have calculated the Laplacian of the experimental static electron density from the results of multipolar refinement 4′ (Table 2). The program *PROP* developed by Souhassou (Souhassou, 1992, Souhassou & Blessing, 1998), based on the topological analysis (Bader & Essen, 1984; Bader, 1990*a*,*b*), has been used in this study. Table 5 gives the topological properties of Si—O, Al—O and Ca^{2+}—O interactions in scolecite to clarify the bond character [distance between the critical point $\mathbf{r}_c$ and the Si, Al and O atoms, Laplacian of the electron density $\nabla^2\rho(\mathbf{r}_c)$, eigenvalues of the Hessian matrix and their ratios $|\lambda_1|/|\lambda_3|$, and electron density peak heights calculated at the critical points]. Some systematic features are found in Table 5 for Si—O, Al—O and Ca^{2+}—O bonds: the ranges of $\rho(\mathbf{r}_c)$ and $\nabla^2\rho(\mathbf{r}_c)$ values are, respectively, 0.9–1.2 e Å^{-3}, 15–21 e Å^{-5} for Si—O, 0.5–0.7 e Å^{-3}, 13–16 e Å^{-5} for Al—O, and 0.12–0.21 e Å^{-3}, 2.4–4.6 e Å^{-5} for Ca^{2+}—O bonds. We also observe in Table 5 that the bond critical points are slightly closer to the O atoms in Si—O bonds (less than 0.70 Å) than in Al—O bonds (greater than 0.76 Å). The electron peak height in Si—O (∼1 e Å^{-3}) is 30% higher than those observed in Al—O links, showing a more pronounced electron concentration in the Si—O bond. The electron density peak height at the critical point in the Si—O bond is in good agreement with the experimental values of 0.94–1.01 e Å^{-3} for danburite (Downs & Swope, 1992) and 1.1 e Å^{-3} found for coesite by Downs (1994). In scolecite the positive curvature corresponding to the λ_3 eigenvalue of the Hessian matrix is much larger for the

Table 6. *The diagonal elements of the hat matrix (leverages H_{ii}) and weighted residuals ($|K^{-1}|F_o| - |F_c||/\sigma(|F_o|)$) of the pertinent data in the determination of the net atomic charges in scolecite*

Reflections (*hkl*)	Constrained refinement (refinement 4 in Table 2) Leverages H_{ii}	Weighted residuals	Non-constrained refinement (refinement 4′ in Table 2) Leverages H_{ii}	Weighted residuals
$\bar{1}53$	0.040	8.20	0.084	4.40
020	0.004	14.96	0.854†	0.86
191	0.030	3.99	0.063	2.37
242	0.060	4.43	0.179	2.16
331	0.068	4.75	0.223	0.06
731	0.135	3.05	0.163	1.09
911	0.013	3.34	0.029	1.02

† Abnormal reflection.

Si—O bond than for the Al—O link, indicating a larger kinetic energy density in the direction of the bond path for Si—O. However, the negative curvatures corresponding to λ_1 and λ_2 are also greater in magnitude for the Si—O bond compared with the Al—O bond. Consequently, the ratios $|\lambda_1|/|\lambda_3|$ of these eigenvalues of $\sim$0.22 for Si—O and 0.19 for Al—O are not very different. Therefore, it is not easy to give a straightforward interpretation of the results in terms of relative ionicity when the Si and Al atoms form a bond with the O atoms. At this stage of the investigation of aluminosilicate materials, we can only estimate the Si—O and Al—O links as bonds of mixed ionic–covalent nature. Furthermore, a lack of comparable theoretical calculations or other experimental results on Si—O—Al links in different geometries is to be noted.

3.4. *Kappa refinements and atomic net charges in scolecite*

In order to obtain atomic net charges which are not dependent on the atomic radial functions $R_{n_l}(r)$ [(1) and (2)], a kappa refinement (Coppens *et al.*, 1979) was performed: at the convergence of the multipolar model refinements all the multipole populations were set to zero and a kappa refinement was carried out in order to derive the atomic charges from the X-ray diffraction data. In this refinement the electronic density of (1) is restricted to

$$\rho(\mathbf{r}) = \rho_{\text{core}}(r) + P_{\text{val}}\kappa^3\rho_{\text{val}}(\kappa r), \qquad (12)$$

where ρ_{core} is the core electron density, which is supposed to be non-perturbed, and the net atomic charge is related to the P_{val} parameter values. The lack of information in the data on the diffuse valence shell of Ca^{2+} (the 4*s* scattering factor of Ca^{2+} at $\sin\theta/\lambda = 0.10$ and $0.15\ \text{Å}^{-1}$ is 0.202 and −0.015 e, respectively) imposes the charge to be fixed at 2+ for this cation in scolecite and thus we kept a 2− charged framework in the kappa refinements. This negative charge was shared at the beginning of the kappa refinement among the O atoms connected to Si and Al.

In order to have reliable P_{val} values we have analysed carefully the data using the hat matrix method described in §2.4. At the end of the multipolar refinements (numbers 4 and 4′ in Table 2) we have performed kappa refinements (numbers 5 and 5′ in Table 2) and calculated the diagonal elements of the prediction matrix, *i.e.* the leverages H_{ii} with respect to the P_{val} parameters (15 parameters in the unconstrained refinement and 8 parameters in the constrained refinement). In the natrolite-like constrained refinement (number 5 in Table 2) and according to the criterion of Velleman & Welsh (1981), 201 observations had their leverages greater than $3n/m$, where $n = 7$ (number of the refined P_{val}'s of the framework atoms minus 1 because of the electroneutrality constraint) and $m = 6610$ reflections. As expected for a valence parameter, the maximum $\sin\theta/\lambda$ value for these 201 observations did not exceed $0.4\ \text{Å}^{-1}$. The most influential reflections are 111 ($H_{ii} = 0.45$), 420 ($H_{ii} = 0.42$) and 240 ($H_{ii} = 0.32$). Since we used a weighted least-squares fit, the weighted residuals $|e_i|/\sigma(|F_{o,\text{h}_i}|) = |K^{-1}|F_{o,\text{h}_i}| - |F_{c,\text{h}_i}||/\sigma(|F_{o,\text{h}_i}|)$ were chosen to locate the eventually aberrant observations. Table 6 gives the list of the seven reflections which had the higher weighted residuals in the constrained refinement. We note that the more influential reflections, such as 111 (weighted residual = 0.50) or 420 (weighted residual = 1.80; not reported in Table 6), do not bear any aberration and surprisingly the seven reflections reported in Table 6 have not, in turn, the highest leverages. Then the statistical analysis was performed at the end of the unconstrained refinement (number 4′ in Table 2) over the P_{val} parameters and gave 212 influential reflections. Table 6 shows that the seven reflections of the first analysis do not have high weighted residuals compared with refinement 5, but the 020 reflection has an abnormal leverage (0.85) and a very low deviation. We have to note that this critical 020 reflection in scolecite is forbidden in natrolite, because of the supplementary *d*-glide mirror perpendicular to **a**. Surprisingly, the other forbidden reflections in natrolite, such as 024, 042 and 060, and those observed in scolecite do not present any aberration; their weighted residuals are 0.8, 1.2 and 0.9, respectively. Moreover, a refinement, not reported here, against all the 6610 data, except for

Table 7. *κ, P_{val} and atomic net charges q obtained by kappa refinements 5′ and 6 (Table 2)*

Refinement		5′			6		
Atoms	κ	P_{val}	q	κ	P_{val}	q	Differences of net charges 5′−6
Si1	1.16 (3)	2.52 (13)	1.48 (13)	1.18 (3)	2.33 (13)	1.67 (13)	−0.19 (13)
Si2	1.31 (4)	1.70 (13)	2.30 (13)	1.25 (4)	1.91 (14)	2.09 (14)	0.21 (14)†
Si3	1.23 (3)	2.25 (14)	1.75 (14)	1.25 (3)	2.20 (14)	1.80 (14)	−0.05 (14)
Al1	1.53 (11)	0.70 (11)	2.30 (11)	1.55 (7)	1.05 (12)	1.95 (12)	0.35 (12)†
Al2	1.36 (5)	1.49 (13)	1.51 (13)	1.50 (8)	1.06 (12)	1.94 (12)	−0.43 (13)†
O1	0.946 (6)	6.85 (8)	−0.85 (8)	0.934 (6)	7.15 (9)	−1.15 (9)	−0.30 (9)†
O2	0.910 (6)	7.69 (9)	−1.69 (9)	0.924 (6)	7.39 (9)	−1.39 (9)	0.30 (9)†
O3	0.947 (6)	7.28 (8)	−1.28 (8)	0.939 (6)	7.31 (8)	−1.31 (8)	0.03 (8)
O4	0.922 (6)	7.22 (8)	−1.22 (8)	0.925 (6)	7.21 (8)	−1.21 (8)	−0.01 (8)
O5	0.937 (6)	7.22 (9)	−1.22 (9)	0.932 (6)	7.31 (9)	−1.31 (9)	0.09 (9)
O6	0.949 (6)	7.08 (8)	−1.08 (8)	0.947 (6)	6.95 (8)	−0.95 (8)	−0.13 (8)
O7	0.965 (6)	6.70 (8)	−0.70 (8)	0.945 (6)	7.00 (9)	−1.00 (9)	0.30 (9)†
O8	0.951 (6)	7.08 (7)	−1.08 (7)	0.952 (6)	7.00 (7)	−1.00 (7)	−0.08 (7)
O9	0.960 (6)	6.89 (7)	−0.89 (7)	0.961 (6)	6.89 (7)	−0.89 (7)	0.00 (7)
O10	0.923 (6)	7.34 (8)	−1.34 (8)	0.933 (6)	7.24 (8)	−1.24 (8)	−0.10 (8)
Ca	1.00	0.00	2.00	1.00	0.00	2.00	0.00
O*w*1	0.988 (8)	6.33 (8)	−0.33 (8)	0.996 (8)	6.31 (8)	−0.31 (8)	−0.02 (8)
H11	1.16	0.98 (5)	0.02 (5)	1.16	0.96 (5)	0.04 (5)	−0.02 (5)
H12	1.16	0.70 (5)	0.30 (7)	1.16	0.74 (7)	0.26 (7)	0.04 (7)
Ow2	0.970 (8)	6.49 (8)	−0.49 (8)	0.959 (7)	6.63 (8)	−0.63 (8)	0.14 (8)†
H21	1.16	0.75 (5)	0.25 (5)	1.16	0.60 (5)	0.40 (5)	−0.15 (5)†
H22	1.16	0.76 (5)	0.24 (7)	1.16	0.78 (7)	0.22 (7)	0.02 (7)
O*w*3	0.951 (7)	6.96 (8)	−0.96 (8)	0.952 (7)	6.96 (8)	−0.96 (8)	0.00 (8)
H31	1.16	0.51 (6)	0.49 (6)	1.16	0.51 (6)	0.49 (6)	0.00 (6)
H32	1.16	0.54 (5)	0.46 (7)	1.16	0.54 (7)	0.46 (7)	0.00 (7)

† The highest net charge differences between the refinements 5′ and 6.

the 020 reflection which bears the highest H_{ii} value (0.85), shows that this unique observation provides the main uncertainty to the refined parameters.

We have carried out a non-constrained kappa refinement (number 6 in Table 2) without the seven reflections given in Table 6. The values obtained at the convergence for κ, P_{val} and atomic net charges are reported in Table 7. In both refinements 5′ and 6 (Table 2) the κ parameters are higher than unity for the Si and Al atoms, revealing the contraction of their electronic valence shells. The contraction of the Al atoms seems, however, overestimated (on average κ = 1.4) compared with that of the Si atoms (on average κ = 1.2). The O atoms have κ-parameter values between 0.90 and 0.96, showing, as expected for electronegative species, a slight expansion of their electronic clouds. Therefore, we note that there is a consistency for these contraction–expansion κ parameters between the two refinements. On the other hand, P_{val} and atomic net charges are not consistent in refinements 5′ and 6. The last column of Table 7 gives the differences between the atomic net charges obtained in the last cycles of the two refinements. The more important change of P_{val} parameters is larger than 0.4 electrons (*i.e.* more than 3 estimated σ's) and concerns Al2. The main feature is that the net charges become almost equal for the pairs (Si2, Si3), (Al1, Al2) and (O1, O2) in refinement 6. Thus, only seven reflections, detected by the hat matrix, are influential reflections among the 6610 observations; this number of reflections (seven) is too small to differentiate between the symmetrically non-equivalent atoms in scolecite. Therefore, it is more reasonable to consider the kappa refinement 6 in Table 2 as best for the estimation of the atomic net charges in scolecite. Applying the hat matrix method to natrolite (Ghermani *et al.*, 1996), no aberration appears in the X-ray data.

In order to illustrate the charge repartition on the atoms of scolecite we have reported the values obtained from refinement 6 in Fig. 5. For a better comprehension of the correlation between the net charges and the environment, the bonds from the calcium ion to the framework and the hydrogen bonds are also drawn in Fig. 5. The atomic net charges in scolecite globally confirm the half ionicity of the atoms in silicate or aluminosilicate materials. This is in good agreement with theoretical calculations on smaller systems (Benco & Smrcok, 1994) or with other experimental methods (Sasaki *et al.*, 1980) for atoms in $[Si(Al)O_4]$ tetrahedra. The values of the charges obtained in scolecite are also qualitatively in accordance with those of our previous study on natrolite (Ghermani *et al.*, 1996). However, the magnitudes of the net charges in scolecite are found to be slightly higher compared with those of natrolite. The silicon net charges in scolecite [+1.67 (13) to +2.09 (14) e] are more scattered than those of natrolite [+1.65 (10) to +1.84 (12) e (Ghermani *et al.*, 1996)]. The difference between the two compounds is more pronounced for the Al atoms: +1.95 (12) e in scolecite against +1.51 (11) e in natrolite. The charges of the O atoms are, consequently, in relation to the number and

nature of the coordinated metals. The O9, O6 and O8 atoms connected, respectively, to two Si atoms or to one Si and one Al atom bear the lowest charges of −0.89 (7), −0.95 (8) and −1.00 (7) e. The other O atoms linked to the Ca^{2+} cation and/or H atoms from the water molecules have larger net charges ranging from −1.15 to −1.4 e (O2), except for O7 [−1.00 (9) e]. The range of the oxygen charges in natrolite is −0.87 (5) (O5) to −1.21 (5) e (O2). Pauling's second rule, termed the electrostatic valence rule, has been applied to scolecite using the net charges derived from the kappa refinement. With the hypothesis that we take into account the H-atom charges of the water molecules (even though we were not able to calculate a charge transfer on the water molecule), the differences of the net charges from the kappa refinement and those calculated from the sum of electrostatic valences are O1 −0.20, O2 −0.03, O3 −0.02, O4 +0.01, O5 −0.09, O6 −0.06, O7 +0.29, O8 −0.06, O9 +0.05 and O10 −0.12 e. In natrolite the same differences are O1 +0.07, O2 −0.09, O3 −0.07, O4 −0.11 and O5 +0.22 e. As the e.s.d.'s of the O-atom net charges are ∼ 0.08 e, we note an agreement with Pauling's rule of the charge transfer in both scolecite and natrolite. However, Pauling's rule does not take into account long-range Pauling's interactions; therefore, a quantitative agreement cannot be expected.

The financial support of the CNRS and of Université Henri Poincaré, Nancy 1, is gratefully acknowledged. We thank Mr Barian, director of the Musée Minéralogique de l'Université de Paris VI for providing the crystal sample of scolecite. SK and NEG would like to thank Drs N. K. Hansen and E. Espinosa for fruitful discussions and useful comments on the original manuscript.

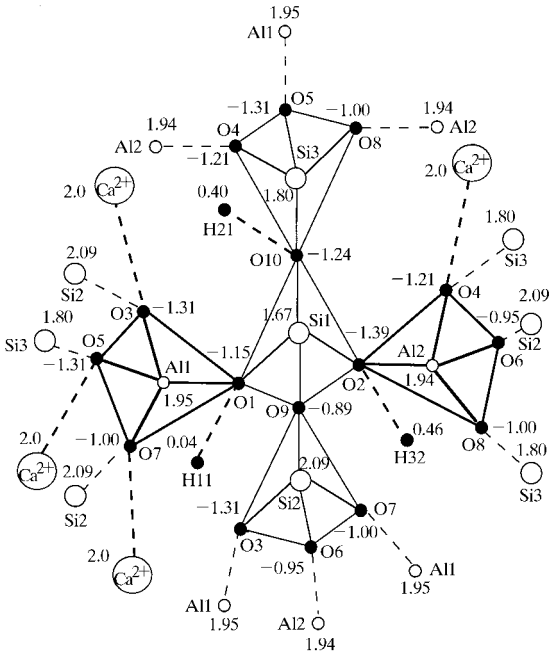

Fig. 5. Schematic representation of the atomic net charges in the scolecite structure from refinement 6.

References

Antoniadis, A., Berruyer, J. & Carmona, R. (1992). *Regression Non Linéaire et Application, Economica*, pp. 1–44. Paris, France.

Bader, R. F. W. (1990*a*). *Atoms in molecules: a Quantum Theory*, pp. 13–52. Oxford: Oxford Science Publications.

Bader, R. F. W. (1990*b*). *Atoms in Molecules: a Quantum Theory*, pp. 275–315. Oxford: Oxford Science Publications.

Bader, R. F. W. & Essen, H. (1984). *J. Chem. Phys.* **80**, 1943–1960.

Bader, R. F. W., MacDougall, P. J. & Lau, C. D. H. (1984). *J. Am. Chem. Soc.* **106**, 1594–1605.

Becker, P. J. & Coppens, P. (1974). *Acta Cryst.* A**30**, 129–147.

Benco, L. & Smrcok, L. (1994). *Phys. Chem. Miner.* **21**, 401–406.

Blessing, R. H. (1987). *Crystallogr. Rev.* **1**, 3–58.

Blessing, R. H. (1989). *J. Appl. Cryst.* **22**, 396–397.

Blessing, R. H. (1995). *Acta Cryst.* A**51**, 33–38.

Clementi, E. & Raimondi, D. L. (1963). *J. Chem. Phys.* **38**, 2686–2689.

Clementi, E. & Roetti, C. (1974). *Atomic Data and Nuclear Data Tables*, Vol. 14, pp. 177–178. New York: Academic Press.

Coppens, P. (1997). *X-ray Charge Densities and Chemical Bonding*. Oxford University Press.

Coppens, P., Guru, T. N., Leung, P., Stevens, E. D., Becker, P. & Yang, Y. W. (1979). *Acta Cryst.* A**35**, 63–72.

Cromer, D. T. (1974). *International Tables for X-ray Crystallography*, edited by J. A. Ibers & W. E. Hamilton, pp. 148–150. Birmingham: Kynoch Press. (Present distributor Kluwer Academic Publishers, Dordrecht.)

Cruickshank, D. W. J. (1949). *Acta Cryst.* **2**, 65–82.

De Titta, G. (1985). *J. Appl. Cryst.* **18**, 75–79.

Downs, J. W. (1994). *Trans. Am. Geophys. Union*, p. 187.

Downs, J. W. & Swope, R. J. (1992). *Phys. Chem.* **96**, 4834–4840.

El Haouzi, A., Hansen, N. K., Le Hénaff, C. & Protas, J. (1996). *Acta Cryst.* A**52**, 291–301.

Enraf–Nonius (1989). *CAD-4 Software*. Enraf–Nonius, Delft, The Netherlands.

Espinosa, E., Lecomte, C., Ghermani, N. E., Devémy, J., Rohmer, M. M., Bénard, M. & Molins, E. (1996). *J. Am. Chem. Soc.* **118**, 2501–2502.

Espinosa, E., Lecomte, C., Molins, E., Veintemillas, S., Cousson, A. & Paulus, W. (1996). *Acta Cryst.* B**52**, 519–534.

Espinosa, E., Souhassou, M., Lachekar, H. & Lecomte, C. (1998). *Chem. Phys. Lett.* **285**, 170–173.

Fälth, L. & Hansen, S. (1979). *Acta Cryst.* B**35**, 1877–1880.

Fedorov, V. V. (1972). *Theory of Optimal Experiments*, translated by W. J. Studen & E. M. Klinko. New York: Academic Press.

Fischer, R. X., le Lirzin, A., Kassner, D. & Rüdinger, B. (1991). *Z. Kristallogr.* Suppl. **3**, 75.

Flack, H. D. (1983). *Acta Cryst.* A**39**, 876–881.

Francl, M. M., Carey, C. & Chirlian, L. E. (1996). *J. Comput. Chem.* **17**, 367–383.

Ghermani, N. E., Bouhmaida, N. & Lecomte, C. (1992). *ELECTROS, STATDENS. Computer Programs to Calculate Electrostatic Properties from High-Resolution X-ray Diffraction*. Internal report URA CNRS 809, Université Henri Poincaré, France.

Ghermani, N. E., Bouhmaida, N. & Lecomte, C. (1993). *Acta Cryst.* A**49**, 781–789.

Ghermani, N. E., Lecomte, C. & Dusausoy, Y. (1996). *Phys. Rev. B*, **53**, 5231–5239.

Gibbs, G. V., Hill, F. C. & Boisen, M. B. Jr (1997). *Phys. Chem. Miner.* **24**, 167–178.

Hamilton, W. C. (1964). *Statistics in Physical Science*. New York: Ronald Press.

Hansen, N. K. & Coppens, P. (1978). *Acta Cryst.* A**34**, 909–921.

Hill, R. J. & Gibbs, G. V. (1979). *Acta Cryst.* B**35**, 25–30.

Hoaglin, D. C. & Welsh, R. E. (1978). *Am. Stat.* **32**, 17.

Joswig, W., Bartl, H. & Fuess, H. (1984). *Z. Kristallogr.* **166**, 219–223.

Kuhs, W. F. (1983). *Acta Cryst.* A**39**, 148–158.

Kvick, Å., Stahl, K. & Smith, J. V. (1985). *Z. Kristallogr.* **166**, 141–154.

Lascaux, P. & Theodor, R. (1986). *Analyse Numérique Matricielle Appliquée à l'Art de l'Ingénieur*, Vol. I. Paris: Masson.

Liebau, F. (1985). *Structural Chemistry of Silicates*. Berlin: Springer Verlag.

McCandlish, E., Stout, G. H. & Andrews, L. C. (1975). *Acta Cryst.* A**31**, 245–249.

Pichon-Pesme, V., Lecomte, C., Wiest, R. & Bénard, M. (1992). *J. Am. Chem. Soc.* **114**, 2713–2715.

Prince, E. & Boggs, P. T. (1992). *International Tables for Crystallography*, edited by A. J. C. Wilson, Vol. C, p. 594. Dordrecht: Kluwer Academic Publishers.

Prince, E. & Nicholson, W. L. (1985). *Structure and Statistics in Crystallography*, edited by A. J. C. Wilson, p. 183. New York: Adenine Press.

Rees, B. (1976). *Acta Cryst.* A**32**, 483–488.

Sasaki, S., Fujino, K., Takénchi, Y. & Sadanaga, R. (1980). *Acta Cryst.* A**36**, 904–915.

Sheldrick, G. M. (1993). *SHELXL*93. *Program for the Refinement of Crystal Structures*. University of Göttingen, Germany.

Souhassou, M. (1992). Am. Cryst. Ass. Meet. Pittsburgh, Pennsylvania, August, Abstract F06.

Souhassou, M. & Blessing, R. H. (1998). *J. Appl. Cryst.* In the press.

Souhassou, M., Espinosa, E., Lecomte, C. & Blessing, R. H. (1995). *Acta Cryst.* B**51**, 661–668.

Souhassou, M., Lecomte, C., Ghermani, N. E., Rohmer, M. M., Wiest, R., Bénard, M. & Blessing, R. H. (1992). *J. Am. Chem. Soc.* **114**, 2371–2382.

Stewart, R. F. (1991). *The Application of Charge Density Research to Chemistry and Drug Design*, edited by G. Jeffrey & J. F. Piniella. NATO ASI Series B, Vol. 250, pp. 63–101. New York, London: Plenum Press.

Thornley, F. R. & Nelmes, R. J. (1974). *Acta Cryst.* A**30**, 748–757.

Val, R. J. van der & Vos, A. (1987). *Acta Cryst.* B**43**, 132–143.

Velleman, P. F. & Welsh, R. E. (1981). *Am. Stat.* **35**, 234–242.

Watkin, D. (1994). *Acta Cryst.* A**50**, 411–437.